Spectroelectrochemical study of the electro-oxidation of ethanol on WC-supported Pt — Part III: Monitoring of electrodeposited-Pt catalyst ageing by in situ Fourier transform infrared spectroscopy, in situ sum frequency generation spectroscopy and ex situ photoelectron spectromicroscopy

Benedetto Bozzini [a,*], Majid Kazemian Abyaneh [b], Bertrand Busson [c], Gian Pietro De Gaudenzi [d], Luca Gregoratti [b], Christophe Humbert [c], Matteo Amati [b], Claudio Mele [a], Abderrahmane Tadjeddine [c]

[a] Dipartimento di Ingegneria dell'Innovazione, Università del Salento, Via Monteroni, I-73100 Lecce, Italy
[b] Sincrotrone Trieste S.C.p.A., ELETTRA, s.s. 14 km 163.5 in Area Science Park, 34012 Basovizza, Trieste, Italy
[c] Univ. Paris-Sud, Laboratoire de Chimie Physique, CNRS, Bâtiment 201 Porte 2, 91405 Orsay, France
[d] Films S.p.a. (Società per azioni), v. Megolo 2, I-28877 Anzola d'Ossola, Italy

HIGHLIGHTS

- ► WC-supported electrodeposited Pt shows superior ethanol electro-oxidation activity.
- ► In situ FTIR and SFG provide complementary molecular information on catalyst ageing.
- ► In situ FTIR and SFG pinpoint multiplicity of CO adsorption sites on WC-supported Pt.
- ► Potential-dependent coadsorption of acetate, ethanol and CO is affected by ageing.
- ► SPEM revealed chemical state distribution of Pt and W as a result of catalyst ageing.

GRAPHICAL ABSTRACT
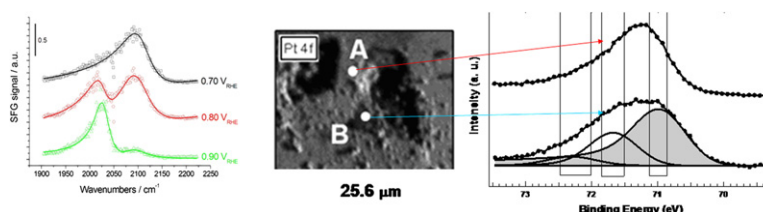
ARTICLE INFO

ABSTRACT

In view of improved durability, the study of electrocatalyst supports for PEMFCs alternative to carbon is raising notable research interest. In this paper we investigated the oxidation of ethanol on WC-supported electrodeposited Pt, in pristine and aged conditions by: (i) electrochemical measurements, (ii) in situ spectroscopy (FTIR and sum-frequency generation spectroscopy (SFG)) carried out during the electro-oxidation of ethanol and (iii) ex situ synchrotron-based space-resolved photoelectron spectroscopy (SPEM). The complementarity of FTIR and SFG allows an insightful understanding of the electrochemical interface as a function of applied potential and catalyst ageing. In situ FTIR and SFG revealed adsorbed acetate and ethanol, in addition to linearly and bridge-bonded CO and solution-phase CO2. The Stark tuning of CO indicates that it is less strongly bonded to aged electrodes. Quantitative analysis of potential-dependent FTIR and SFG spectra reveals that the population of adsorption sites for CO, acetate

* Corresponding author. Tel.: +39 (0)832 297323; fax: +39 (0)832 297111.
E-mail address: benedetto.bozzini@unisalento.it (B. Bozzini).

WC
SFG
SPEM

and ethanol changes with ageing and correlates with loss of catalytic activity. Changes in catalyst morphology as well as Pt and WC chemical state have been pinpointed by SPEM: electrodeposited Pt nanoparticles tend to agglomerate and the distribution of oxidised and reduced forms of Pt and W correlates with the attack of the catalyst support.

1. Introduction

One of the technological barriers crucially inflating the time-to-market of real consumer devices implementing proton exchange membrane fuel cells (PEMFC) is their durability. Among other crucial durability issues, it is worth emphasising the stability of the catalyst/substrate system, that tends to be jeopardised by several processes related to PEMFC operation. In fact, in the literature, in addition to the insightfully investigated CO-poisoning problems, other complex and poorly understood degradation modes have been reported, including: (i) Pt dissolution and reprecipitation [1–3]; (ii) agglomeration of nanoparticles [4–10], (iii) carbon-support corrosion [11–17]. In particular, the unanimously recognised degradation of universally used carbon-supported Pt-based catalysts, is fostering research on novel catalyst-support materials, that might exhibit better stability towards corrosion, catalyst dissolution, surface migration of Pt and agglomeration of Pt and Pt-alloy nanoparticles. Among promising support materials, WC has recently received considerable attention. In fact, this material features suitable electronic conductivity, notable resistance to acidic environment, some degree of activity for H_2 oxidation, low cost, high thermal and chemical stability as well as excellent mechanical properties, that are desirable for applications where fretting degradation is important, such as automotive ones [18–29]. Furthermore, the addition of WC to Pt [21], Pt–Ru [21], Pd [27,29] and AuPd [28] catalysts has been shown to improve the tolerance to CO during ethanol oxidation. It is also worth noting that Pt–WC and Pt–WC/C have been proposed as O_2 electro-reduction catalysts [26].

In the two previous papers of this series (Parts I and II) we studied the behaviour of WC-supported Pt black, while in the present work (Part III) we are concentrating on electrodeposited Pt. As analytical tools, in this work we have used in situ FTIR and SFG – with the same approach proposed in Refs. [18,19] – and in addition we have resorted to synchrotron-based photoelectron microspectroscopy for high-resolution, space-resolved chemical state speciation [30,31]. In Refs. [18,19,30,31], we have investigated the degradation of the catalytic performance of Pt-based materials by a range of spectroscopic tools. Of course, pure Pt is not a state-of-the-art electrocatalyst for ethanol oxidation – that typically adopts alloyed Pt, such as Pt–Ru –, but – as emphasised in [18,19] – pure Pt can be regarded as a benchmark material for the assessment of the behaviour of the novel WC support. In particular, within the scope of this project, we have considered Pt black as a standard [18,19] and electrodeposited Pt nanoparticles (this work) as a more flexible approach, especially intended as the possible preparation method of choice for nanostructured supports. It is well known that catalyst layers can be applied by several techniques, such as impregnation, painting and spraying and electrodeposition. Among these approaches, electrodeposition is considered an appealing and innovative option, since it allows accurate control of particle size and catalyst distribution over the substrate [32]. Although electrodeposition of Pt has been studied by a number of researchers, only a few works have studied the electrodeposition for the preparation of the catalyst layers for PEMFCs [33–37]. In particular, the galvanostatic preparation of a Pt catalyst layer onto carbon cloth was studied by direct current [33] and pulse plating from a chloroplatinic acid bath [33,38]. An electrodeposition method consisting of a two-step procedure and involving the impregnation of platinum ions into a preformed catalyst layer, followed by a potentiostatic reduction was proposed in Ref. [39], demonstrating the feasibility of a cation-exchange/electroreduction. Moreover the effect of hydrophilic and hydrophobic sublayers on the electrodeposited platinum catalyst and on the resulting fuel cell performance was investigated in Ref. [40].

As far as XPS studies of electrocatalysts are concerned, this method is widely documented in the literature, typically in order to characterise electrocatalysts in the as-fabricated conditions. Regarding catalyst degradation, [15] reports XPS measurements of Pt/C electrocatalysts before and after 10,000 potential cycles between 0.6 and 1.2 V_{RHE}: an increase of the relative amount of Pt(0)–Pt(II) has been found, interpreted in terms of Pt dissolution and redeposition, resulting in Ostwald ripening. Ref. [8] investigated by XPS the effects of repeated application of potential steps (from 0.60 or 0.85 to 1.4 V_{RHE}) and prolonged potentiostatic polarisation (at 1.2 and 1.4 V_{RHE}) on the degradation of Pt/C: O and C were found to increase and the C peak has been shown to shift towards the formation of oxidised C species. Similar conclusions have been reached in Ref. [41] that applied 800 potentiodynamic cycles between 0 and 1.5 V_{RHE}. Ref. [42] reports on the degradation of a Pt–Ru catalyst implemented in a MEA, caused by cell reversal during starvation; quantitative elemental analysis disclosed changes in C and O content and, in particular, highlighted the decrease of Pt content in the catalyst alloy.

Even though the full spectrum of durability problems related to electrocatalyst–support interactions is still far from being understood and, of course, we aimed just at a specific selection of model materials and ageing processes, this work is intended to contribute to the molecular-level understanding of such processes as well as to the rationalisation of the behaviour of WC as a novel electrocatalyst support. It is also worth recalling that the level of physico-chemical insight achieved in this work, has been possible thanks to a multi-technique approach relying on spectroscopic information that directly addresses many observables involved in the degradation processes, at variance with the integral approaches commonly adopted in similar studies.

2. Experimental

2.1. Electrodes and electrolytes

A sintered (93% of theoretical density) WC cylinder of diameter 1 cm and height 1 cm was provided by Korea Tungsten TaeguTec Ltd. The sample was characterised by XRD and proved to be single-phase, disoriented diffractometrically pure WC (Fig. 1). Electrodeposition of Pt was carried out on cross-sections of the WC cylinder polished with diamond pastes down to 0.3 μm by Films S.p.a., v. Megolo 2, I-28877, Anzola d'Ossola, Italy. The Pt-plating bath was an aqueous solution of composition: 5 mM $PtCl_2$.0.5 M H_2SO_4. Electrodeposition baths as well as all the other solutions employed water of resistivity > 18 MΩ cm, prepared with a Millipore system. Details of the electrodeposition process are provided
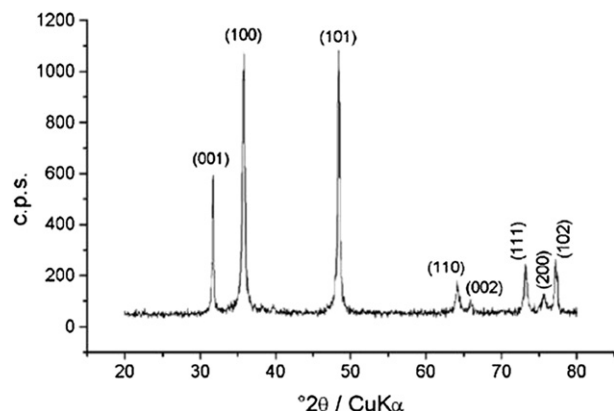
Fig. 1. X-ray diffractogram of sintered WC.

in Section 3.1. Electro-oxidation experiments were carried out in aqueous solutions of composition: 0.1 M EtOH, 0.1 M HClO$_4$. Artificial ageing of the electrodes was performed as described in Ref. [19].

2.2. Electrochemical and spectroelectrochemical methods

Potentiostatic and voltammetric measurements were performed with an AMEL 5000 programmable potentiostat. For electrodeposition work we used an Ag–AgCl reference electrode, while for electrocatalytic work the reference electrode was an RHE, all potentials reported below are referenced to the RHE scale. A scan rate of 0.05 V s^{-1} has been employed for the measurements of cyclic voltammetries. Subtractively normalised FTIR measurements were carried out with the equipment and data-analysis methods detailed in Part II of this work [19]. Sum Frequency Generation spectroscopy (SFG) measurements in the IR wavenumber ranges 1300÷1430 and 1900÷2225 cm^{-1} have been carried out with the IR Free Electron Laser (IR-FEL) and Optical Parametric Oscillator (OPO) described in Ref. [18]: the same data analysis method and modelling algorithms have been employed. Compositional mapping and high lateral-resolution XPS measurements were carried out by using the Scanning Photo-Electron Microscope (SPEM) based at the ESCA (Electro Spectroscopy for Chemical Analysis) microscopy beamline at the ELETTRA synchrotron radiation facility located in Trieste, Italy. Spatially resolved photoemission spectra of selected regions and chemical

maps were acquired with 200 meV energy resolution by using 670 eV photon energy. More details on this microscope and on the beamline can be found in Ref. [43]. For data analysis and presentation purposes, the following quantitative treatments have been carried out: (i) the survey spectra have been normalised to the Pt 4f peak; (ii) the energies have been calibrated with respect to the valence band spectra: as the energy reference we used a Pt(111) surface, analysed under the same conditions.

3. Results and discussion

3.1. Pt electrodeposition

Pt electrodeposition on WC substrates has been carried out with the materials detailed in Section 2.1. The cyclic voltammogram recorded for a WC substrate in contact with the Pt electrodeposition bath is shown in Fig. 2A (scan rate 0.05 V s^{-1}): the onset potential for Pt deposition (∼−0.25 V vs. Ag/AgCl) can be clearly identified by varying the cathodic terminal voltage (see red voltammogram). As soon as Pt is deposited, also H$_2$ is evolved at the cathode, as witnessed by the hydrogen oxidation peak visible in the anodic-going scan. The electrodeposition conditions were optimised in view of the achievement of a continuous layer of Pt nanometric crystallites: the ideal procedure proved to be the application of a potential ramp between −0.275 and −0.700 V vs. Ag/AgCl with a scan rate of 0.5 mV s^{-1}: highly repeatable linear sweep voltammograms were recorded, as shown in Fig. 2B. A typical SEM micrograph of electrodeposited Pt in pristine conditions is shown in Fig. 3A.

3.2. Artificial electrochemical ageing

Artificial ageing of the electrodes (see Ref. [19] for details on the protocol) was performed by holding the potential at +0.65 V, within the ethanol oxidation range, but cathodic with respect to the WC oxidation threshold, for 36 h. This ageing process led to remarkable morphological and chemical changes, that have been studied by SEM and SPEM in Section 3.6: the most notable morphological effects are: (i) particle agglomeration on the submicrometric scale and (ii) localised corrosion of WC on the micrometric scale. As commented above, the SEM image of Fig. 3A shows that the surface of as-electrodeposited Pt/WC sample is homogeneous and exhibits a monodisperse granulometry with average size ∼100 nm. After electrochemical ageing
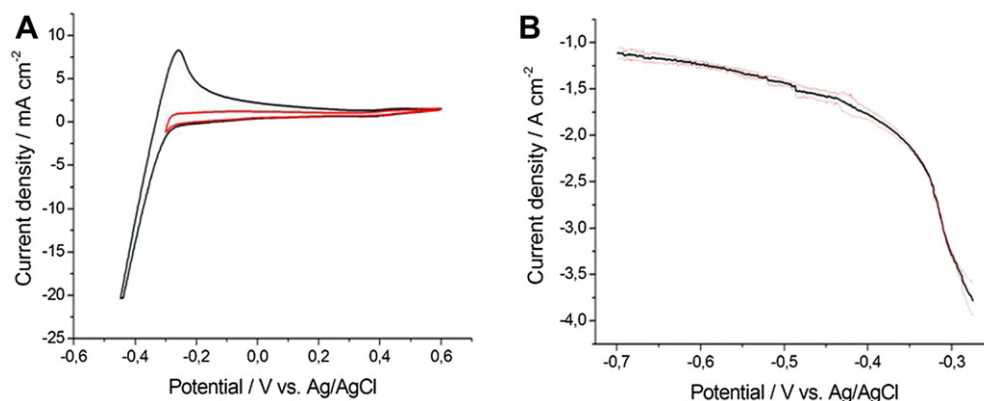

Fig. 2. I–V curves recorded for WC in contact with the aqueous Pt electrodeposition solution of composition: 5 mM PtCl$_2$, 0.1 M H$_2$SO$_4$. (A) Cyclic voltammograms (scan rate 0.05 V s^{-1}) with different cathodic terminal voltages. (B) Linear sweep voltammograms (scan rate 0.5 mV s^{-1}) corresponding to optimised electrodeposition conditions: the thick black line represents the average of three independent experiments and the thin red ones the 1−σ confidence band. (For interpretation of the references to colour in this figure legend, the reader is referred to the web version of this article.)
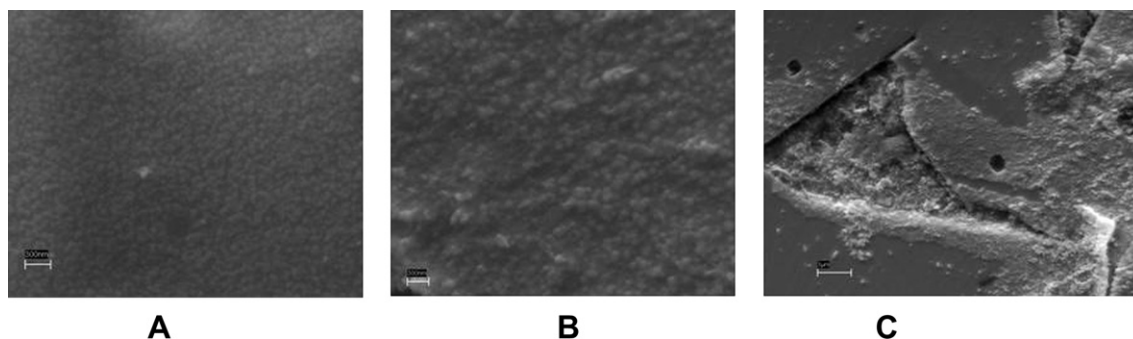
Fig. 3. SEM micrographs of WC-supported electrodeposited Pt catalyst: (A) before cycling (typical, homogeneous morphology), (B, C) after electrochemical cycling. Panel C shows a substrate attack feature, developing by anodic attack.

heterogenerities develop both on the submicrometric scale — corresponding to Pt agglomeration (Fig. 3B) — and on the micrometric scale — deriving from WC corrosion (Fig. 3C) by pitting and transgranular attack (see also Ref. [44]). Corrosion of the substrate was found to have a bearing on the reorganisation and clustering of the Pt particles.

3.3. Cyclic voltammetry

In Fig. 4A, for reference purposes (see also Ref. [18] Fig. 1, [19] first paragraph of Section 3, the corresponding comments and the relevant references), we report the cyclic voltammograms obtained with a bare WC electrode immersed in a 0.1 M $HClO_4$ solution, in the absence and presence of 0.1 M ethanol. According to a common literature protocol (see Ref. [18] and references therein), the voltammograms were recorded between −0.0 V and 1.2 V. We can note that: (i) the oxidation of WC takes place at potentials more anodic than 0.9 V; (ii) a region of hydrogen adsorption is not clearly defined; (iii) the curves recorded without and with added ethanol are very similar. We can conclude that the bare WC electrode does not exhibit any appreciable electrocatalytic behaviour towards ethanol.

The cyclic voltammetry measurements performed at the same electrode, after electrodeposition of Pt are shown in Fig. 4B (0.1 M $HClO_4$), 4-C (0.1 M $HClO_4$ + 0.1 M EtOH, pristine electrode) and 4-D (0.1 M $HClO_4$ + 0.1 M EtOH, aged electrode). When the
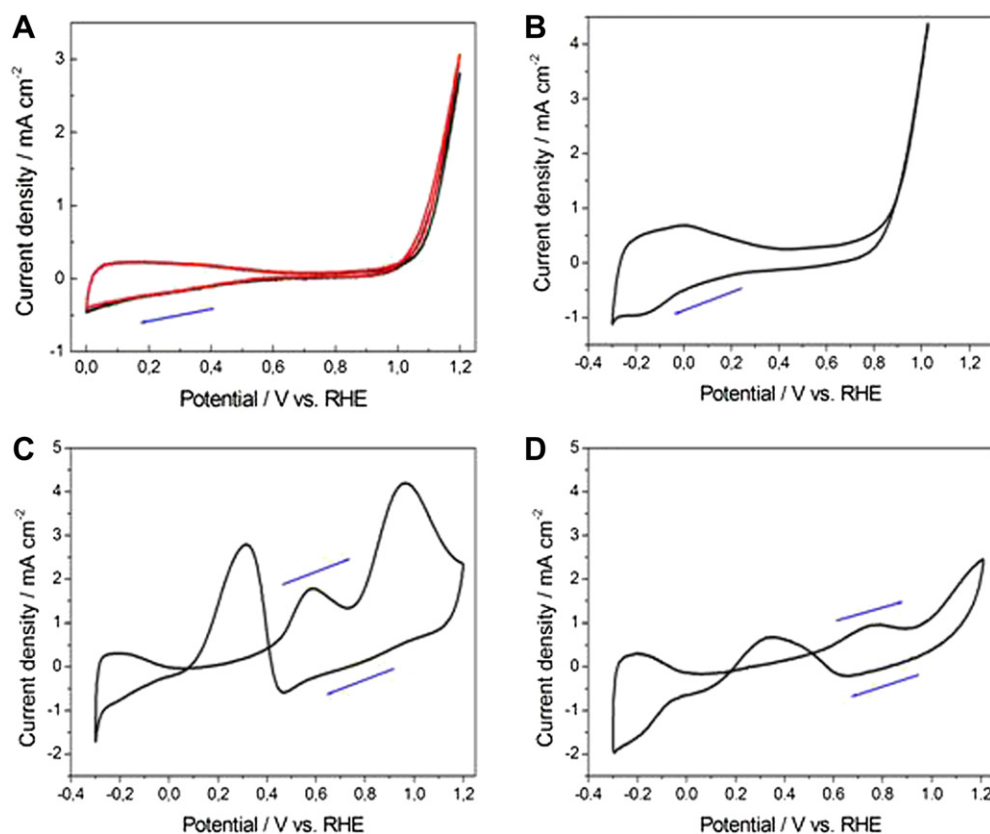

Fig. 4. (A) Cyclic voltammograms obtained with a WC electrode in contact with 0.1 M $HClO_4$ (black line) and 0.1 M $HClO_4$ + 0.1 M CH_3CH_2OH (red line) solutions. (B) Cyclic voltammograms obtained with a WC-supported electrodeposited Pt electrode in contact with a 0.1 M $HClO_4$ solution. (C) Cyclic voltammograms obtained with a pristine WC-supported electrodeposited Pt in contact with a 0.1 M $HClO_4$ + 0.1 M CH_3CH_2OH solution. (D) Same as previous, after ageing. In all cases, the scan rate is 0.05 V s^{-1}. (For interpretation of the references to colour in this figure legend, the reader is referred to the web version of this article.)
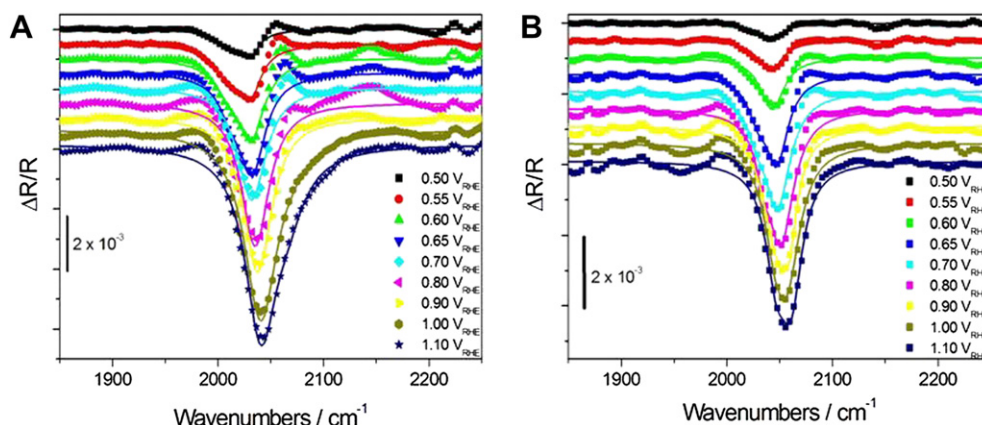
Fig. 5. Potential-dependent in situ FT-IR spectra measured at the indicated potentials on a WC/ECD-Pt electrode in contact with a 0.1 M $HClO_4$ + 0.1 M CH_3CH_2OH solution; reference spectrum measured at 0.05 V_{RHE}. Wavenumbers range corresponding to CO stretching. (A) Pristine sample, (B) aged sample.

functionalised electrode is immersed in the solution containing only 0.1 M $HClO_4$ (Fig. 4B), we observe a voltammetric behaviour that is similar to that of a nanocrystalline Pt electrode in acidic solution, in terms of hydrogen evolution and Pt oxidation. Moreover, a Tafel-type current due to the oxidation of the WC substrate is observed at potentials more anodic than 0.90 V. In the presence of EtOH-containing solution (Fig. 4C), two peaks were observed in the anodic scan, around 0.6 V and 0.95 V. According to the interpretation provided in Ref. [45] – summarising previous mechanistic work on electrochemical EtOH oxidation at Pt-based electrodes – and extended to the case of WC supports in Ref. [18,21], these peaks can be related to EtOH oxidation by: (i) OH_{ads} onto a Pt(I) intermediate state (see in particular Ref. [21] for the specific case of WC support) and (ii) PtO, respectively. We can thus conclude that the behaviour of the WC-electrodeposited Pt system, coherently with our results regarding WC–Pt black [18], in the relevant potential range, shows the typical essential characteristics of Pt-based electrodes. In the case of electroposited Pt, the less anodic peak is centred at the same potential found with WC-supported Pt-black [18], but with a higher current density (c.d.) value; the latter is shifted by 0.1 V in the anodic direction with respect to Pt-black, but the c.d. is a factor of two higher: these features denote better electrocatalytic activity of electrodeposited Pt with respect to Pt-black. Essentially the same voltammetric features are retained after ageing, but the oxidation c.d.s are notably lower and the anodic peaks are shifted to higher potentials. Among the changes due to catalyst ageing, one can also notice a slight activation in the hydrogen UPD region at ca. ~ -0.2 V.

3.4. In situ subtractively normalised FTIR

In situ FTIR was selected for the present research because – owing to its extreme sensitivity to the interfacial conditions of adsorbed CO, combined with the capability of detecting subtle changes in relative surface composition as a function of potential shifts – it is ideal for the monitoring of support-catalyst modifications resulting from prolonged usage. In Part II of this research [19] we have reported cognate results regarding the Pt-black/WC system. Even though the electrocatalytic peculiarities of electrodeposited-Pt/WC system, the novel material proposed in the present work, are extensively discussed and contrasted to Pt-black/WC in the present Section, reference to Figs. 2–5 and Sections 3.1–3.3 of Ref. [19] is recommended for a full appreciation of the differences between the two materials. Applying the protocol of [19], we carried out potentiostatic FTIR measurements by stepping the potential anodically in the range +0.50÷1.10 V. The reference potential for spectral ratioing was set to +0.050 V. We repeated the experiment before and after artificial ageing of the electrodes. The observable spectral patterns found in the two experiments are qualitatively similar to the results of [19] and coherent with the literature [46–54], but electrode ageing gives rise to marked quantitative differences between Pt-black and electrodeposited Pt.

Three chief types of IR bands were measured: (i) adsorbed CO (~ 2050 cm^{-1}), (ii) other ethanol oxidation products (ranges $\sim 1200÷1400$ and $1700÷1750$ cm^{-1}) and (iii) liquid-phase CO_2 (~ 2350 cm^{-1}).
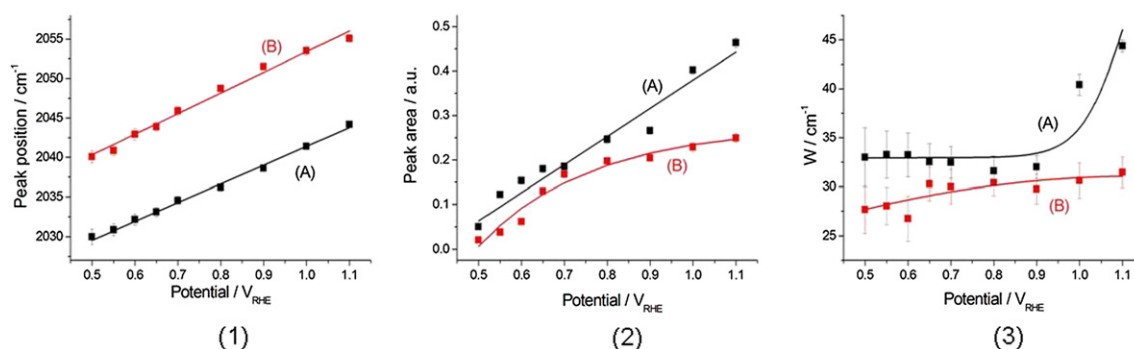

Fig. 6. Lorentzian fit parameters of the linearly adsorbed CO stretching peaks reported in Fig. 5, with respective 95% confidence intervals. (1) Peak position ν_o, (2) peak area A, (3) peak width W. (A) Pristine sample, (B) aged sample.

3.4.1. CO stretching range

In the wavenumber range of the stretching of linearly adsorbed CO ν(CO) ($\sim$2050 cm^{-1}), the prototypical negative band is found, corresponding to the widely-documented ethanol oxidation intermediate. In Fig. 5 we report two sets of potential-dependent spectra for the pristine (A) and aged (B) electrodes. The ν(CO) bands exhibits peak position, Stark tuning (Fig. 6, Panel 1), peak area A (Fig. 6, Panel 2) and peak width W (Fig. 6, Panel 3) that depend on both oxidation potential and ageing conditions. From Panel 1 it can be noticed that, after ageing, the peak position shifts systematically to higher wavenumbers and the Stark tuning is slightly higher (pristine: 23.75 $\pm$ 0.65, $\rho^2 = 0.9948$; aged: 26.15 $\pm$ 1.21 cm^{-1} V^{-1}, $\rho^2 = 0.9853$): both denoting weaker bonding to the surface [55]; it is also worth noting that a higher Stark tuning corresponds to a decrease of CO$_{ads}$ coverage, coherently with the findings of [56]. As expected, the peak area (Panel 2), proportional to surface coverage with CO$_{ads}$, increases with oxidation potential, but after ageing it is lower and less responsive to oxidising conditions. The peak width (Panel 3), essentially related to heterogeneous broadening [57], is higher for the pristine electrode, indicating that several adsorption sites are operative − coherently with the results of Panels 1 and 2, while only specific adsorption sites survive ageing.

It is worth noting that the behaviour of peak position and Stark tuning as a function of ageing is the opposite in Pt black and in electrodeposited Pt: in the former both the peak position and the Stark tuning tend to decrease systematically with ageing [19]. A decrease of the peak area with electrode ageing has also been observed with WC-supported Pt black [19]. Again at variance with the case of Pt black, the peak width of pristine electrodeposited Pt is sensitive to potential, while both types of Pt do not seem to exhibit a definite trend in the aged condition.

The result concerning ν(CO) point to the fact that, while in the case of WC-supported Pt black the evolution of electrocatalyst activity with ageing is related to an increase in CO bonding strength, without a change in the nature of adsorption sites (peak width), in the case of electrodeposited Pt the adsorption strength of CO$_{ads}$ tends to be weakened and the peaks are narrowed as a result of the survival of specific adsorption sites. Of course, the presence of weaker CO-adsorption sites in electrodeposited Pt is a desirable property for the anodic oxidation of alcohols. With both types of Pt, a decrease of active site coverage accompanies ageing.

3.4.2. Wavenumber range 1200÷2000 cm^{-1}

Fig. 7 reports IR spectra measured for the pristine (Panels A and B) and aged (Panels C and D) electrodes, in a wavenumber range containing diagnostic bands corresponding to ethanol and several of its oxidation products. In our spectra we found the following bands: (i) at $\sim$1280 cm^{-1} (Panels A and C, Peak 1), occasionally accompanied by a shoulder corresponding to a band at $\sim$1250 cm^{-1} (Panel C, Peak 5); (ii) at $\sim$1380 cm^{-1} (Panels A and C, Peak 2); (iii) at $\sim$1720 cm^{-1} (Panels B and D, Peak 3) and (iv) at $\sim$1820 cm^{-1} (Panels B and D, Peak 4). According to the literature, Peaks 1−5, can be assigned as follows: (1) C−OH stretching of acetic acid [48]; (2) coupled C−O stretching and OH deformation of ethanol [47,53]; (3) C=O stretching of acetic acid [51]; (4) bridge-bonded CO [51,58]; (5) COH−CH$_3$ combination band that can be assigned to both acetic acid and ethanol [47].

With the pristine electrode, by shifting the potential in the anodic direction, Peaks 1, 3 and 4 forms first and peak 2 increases as the potential grows anodic. This indicates that acetic acid forms and the relative surface coverage with ethanol grow with the oxidation rate. Apart from quantitative details, this behaviour is coherent with that found with WC-supported Pt black [19]. Peak 4 exhibits
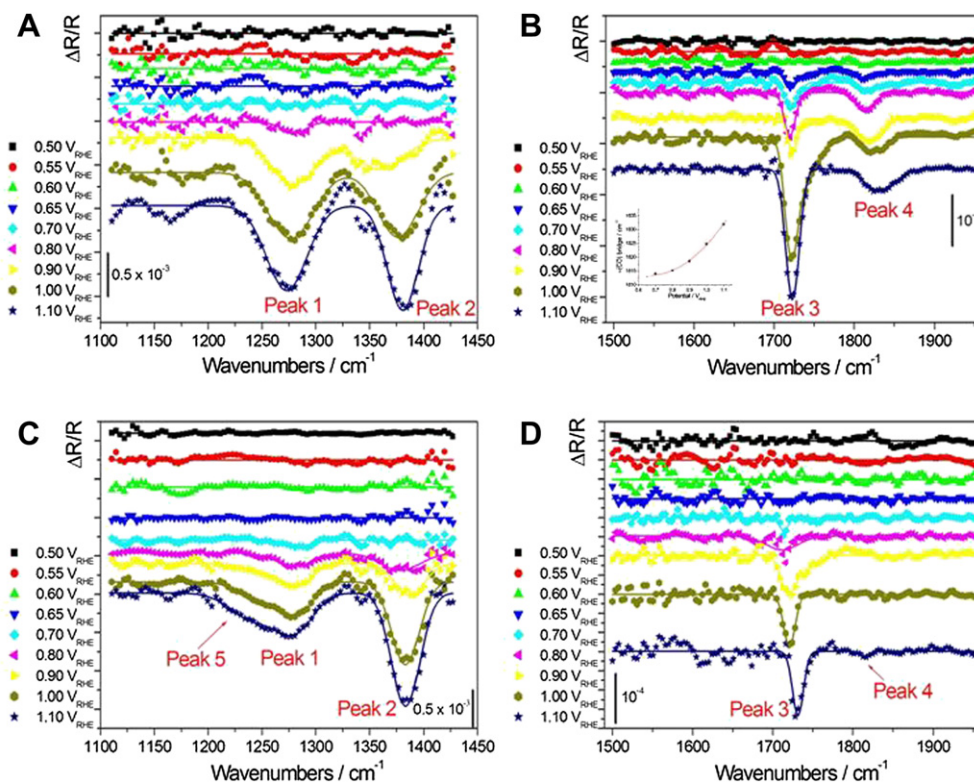

Fig. 7. Potential-dependent in situ FT-IR spectra measured at the indicated potentials on a WC/ECD-Pt electrode in contact with a 0.1 M HClO$_4$ + 0.1 M CH$_3$CH$_2$OH solution; reference spectrum measured at 0.05 V_{RHE}. Wavenumbers range corresponding to diagnostic modes of acetic acid and ethanol. (A, B) Pristine sample, (C, D) aged sample. The inset in Panel B illustrates the Stark tuning of Peak 4.
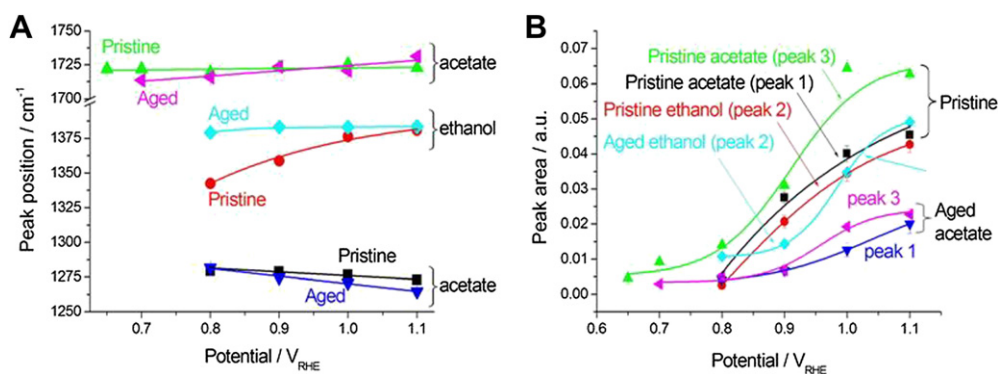
Fig. 8. Lorentzian fit parameters of the peaks reported in Fig. 7, with respective 95% confidence intervals. (A) Peak position ν_o, (B) peak area A. Peak assignments, samples and respective conditions are indicated in the figure.

a parabolic Stark tuning (see inset of Panel B), denoting a potential-dependent type of interaction with the substrate: a detailed discussion of this issue can be found in Ref. [55]. The spectral scenario found with the aged electrode is similar to that corresponding to pristine conditions, apart from three important differences: (i) the surface coverage with ethanol is higher (the relative intensity of Peak 2 with respect to 1 increases), (ii) Peak 4, corresponding to bridge-bonded CO, is hardly visible and Peak 3 exhibits a Stark tuning, denoting stronger bonding of the C=O moiety with the aged Pt surface [19].

In Fig. 8 we report potential-dependent peak positions and areas for pristine and aged electrodes. It can be noticed that both ethanol and acetate peaks exhibit a Stark tuning, − each with a specific direction, proving that these bands correspond to adsorbed moieties. Ageing affects the entity of the Stark shift. An insightful mechanistic discussion of the reaction path and the way it is modified by ageing is beyond the scope of this work, but the diagnostic value of these spectroscopic observables cannot be over-emphasised. Coherently with our results on WC-supported Pt black, the peak positions of acetate and ethanol are affected by electrocatalyst ageing. This finding can be explained with a decrease of active site surface concentration upon ageing, resulting in the decrease of partial oxidation of ethanol and hence increase of ethanol at the interface, in accord with our previous study on WC-supported Pt black, as well as with our conclusions of Section 3.4.1. The peak widths W do not exhibit a measurable potential dependence, but are in some cases affected by ageing: Peak 1 (acetate): pristine 36.17 ± 8.31 cm^{-1}, aged 45.31 ± 9.17 cm^{-1}; Peak 2 (ethanol): pristine 26.66 ± 5.36 cm^{-1}, aged 31.44 ± 5.57 cm^{-1}; Peak 3 (acetate): pristine 14.77 ± 4.18 cm^{-1}, aged 18.04 ± 3.57 cm^{-1}.

Ageing seems to increase the width of both acetate and ethanol bands, the effect being more marked for the former.

3.4.3. Aqueous-phase CO_2

The band at 2343 ± 1 cm^{-1} corresponds to the asymmetric stretching of the O−C−O group of solution-phase CO_2: its peak position is independent on electrode ageing (Fig. 9). A limited, but quantitatively significant change of peak width is found between pristine and aged conditions: 9.77 ± 1.37 and 10.12 ± 0.66 cm^{-1}, respectively. Coherently with the literature ([47] and references therein contained), the increasing width with electrode ageing highlights changes in electroactivity. Nevertheless, the change in width for WC-supported electrodeposited Pt is notably less than that found with WC-supported Pt black: 8.5 ± 3.9 cm^{-1} for pristine conditions and 16.1 ± 7.5 cm^{-1} after ageing.

3.5. In situ SFG

In the present research we resorted to SFG spectroscopy, in order to complement FTIR information, for three chief reasons: (i) extreme interfacial sensitivity; (ii) single-state capability; (iii) responsivity to both the vibrational and electronic structure of the electrochemical interface: this combination of highlights makes SFG ideal for the identification of support-catalyst interactions and in particular of their modifications, such as the ageing issues we are interested in this work. In Part I of this investigation [18] we have reported results obtained for the Pt-black/WC system and in this Section we discuss the behaviour of the novel electrodeposited-Pt/WC system and compare it to that of Pt-black/WC. For a more
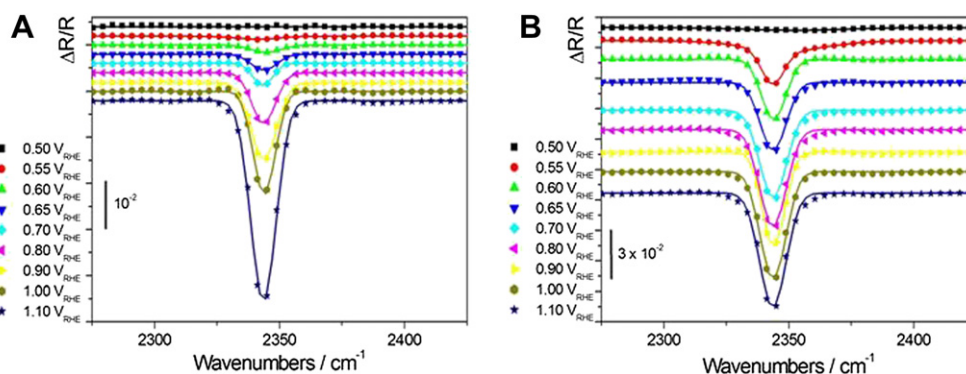

Fig. 9. Potential-dependent in situ FT-IR spectra measured at the indicated potentials on a WC/ECD-Pt electrode in contact with a 0.1 M HClO$_4$ + 0.1 M CH$_3$CH$_2$OH solution; reference spectrum measured at 0.05 V_{RHE}. Wavenumbers range corresponding to CO$_2$. (A) Pristine sample, (B) aged sample.

insightful understanding of the relative differences of the two materials we suggest to refer to Figs. 2–5 and Section 3.2 of [18].

A sequence of SFG spectra was acquired between 0.5 and 1.1 V, by shifting the potential towards anodic values in steps of 0.1 V. Apart from the initial spectrum, that was obtained by pre-polarising the electrode at 0.5 V for 1 h, the potential was set at the desired value just before the acquisition of a spectrum that took ∼20 min.

3.5.1. CO stretching range

The spectra corresponding to the CO stretching range are shown in Fig. 10: panels A and B correspond to pristine and aged conditions, respectively; panels C and D report a selection of data derived from panels A and B highlighting spectral details. CO_{ads} bands are found in the whole investigated potential range and notable qualitative differences can be observed, resulting from both applied polarisation and ageing. The most notable feature is the presence of two peaks at ∼2010÷2030 (peak I) and 2060÷2120 cm^{-1} (peak II) − corresponding to on-top adsorbed CO [59–64] − and (ii) a smaller one at ∼2200 cm^{-1} (peak III), that can be assigned to weakly bonded on-top CO. The presence of three bands for on-top adsorbed CO denotes the fact that different adsorption sites and configurations are present in our catalyst: the lower-wavenumber one dominates in the pristine and aged samples at lower anodic polarisations. The highest frequency mode is very weak with pristine electrodes and almost absent after ageing. In fact, this band can be observed only with a pristine sample at positive potentials, typically above 0.8 V, corresponding to the onset of the direct electrooxidation of ethanol (see the minimum between the two anodic voltammetric peaks in Fig. 4C). Such a high frequency of the CO stretching is correlated to a softening of the adsorbed CO−Pt interaction due to the co-adsorption with another oxidised species, on-top of a the same atom. This coadsorption mode has

been previously observed for hydrogen on platinum electrode in acidic solution, at potential close to the onset of hydrogen evolution [61] and assigned to the adsorbed precursor of the hydrogen evolution. The relative resonator strengths and Stark tuning values are profoundly affected by ageing: the corresponding fit parameters are reported in Fig. 11 (panels A and C: pristine catalyst; panels B and D: aged catalyst). The Stark tuning of Peak I is notably increased by ageing, while that of Peak II is decreased (Panels A and B). It is worth noting that different absolute values of the Stark tuning were found by FTIR and SFG: this is coherent with the results of [65] and due to the different degree of surface sensitivity of the two techniques, thus highlighting their complementarity; notwithstanding the quantitative differences, an increase is found for Peak I − dominating at high anodic polarisations − by both techniques. As far as resonator strengths are concerned (Panels C and D), one can notice that a maximum is found both in pristine and aged conditions: in the former case Peak I dominates over the whole investigated potential range and the maximum is found at 0.9 V, while in the latter one, Peak II prevails at low anodic overvoltages while Peak I is higher at more oxidising potentials. The maximum intensity for Peak I is found at 0.9 V also after ageing, while that of Peak II is measured at 0.75 V. The potential dependence of the peak intensities found by SFG is coherent with the results of FTIR spectroscopy reported in Section 3.4.1 and the same comments apply here too. The widths of the two peaks are slightly different − denoting a different degree of heterogeneous broadening for the respective on-top adsorption sites − they are not measurably affected by the applied potential, while ageing has an effect: peak I pristine, 29.86 ± 6.99 cm^{-1}, aged, 21.98 ± 3.54 cm^{-1}; peak II pristine, 35.62 ± 3.62 cm^{-1}, aged 38.16 ± 4.91 cm^{-1}. The behaviour of the width of Peak I is coherent with that of the dominating FTIR peak and the same explanations proposed in Section 3.4.1 apply here as well.
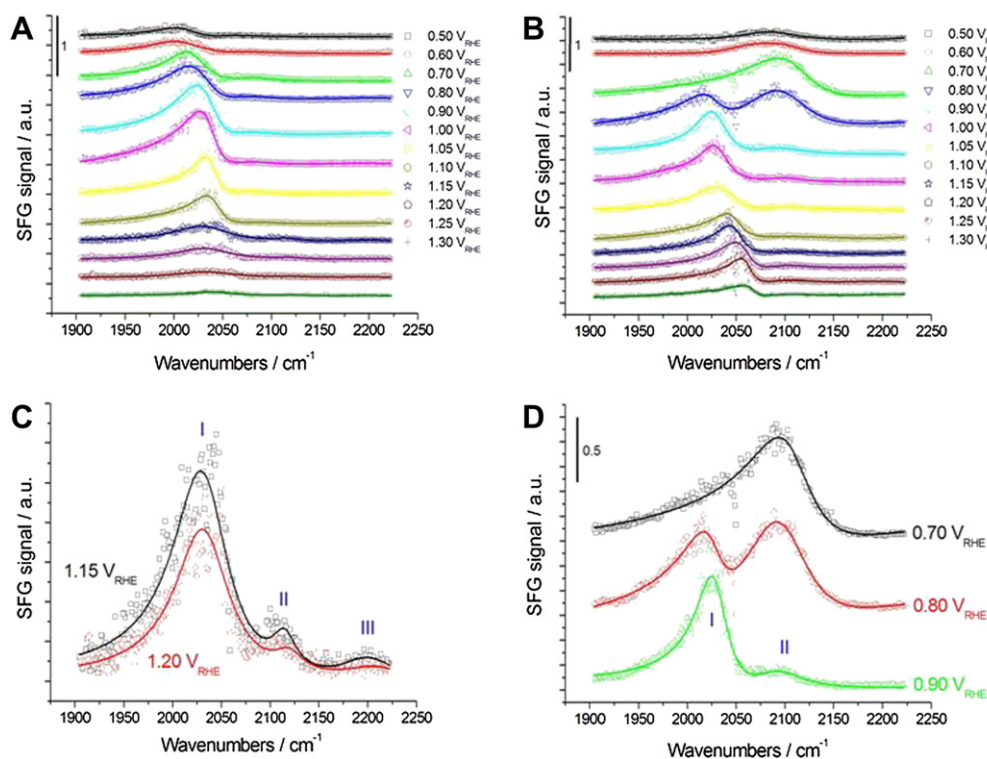

Fig. 10. Potential-dependent in situ SFG spectra measured at the indicated potentials on a WC/ECD-Pt electrode in contact with a 0.1 M $HClO_4$ + 0.1 M CH_3CH_2OH solution. Wavenumbers range corresponding to adsorbed CO. (A, C) Pristine sample, (B, D) aged sample.
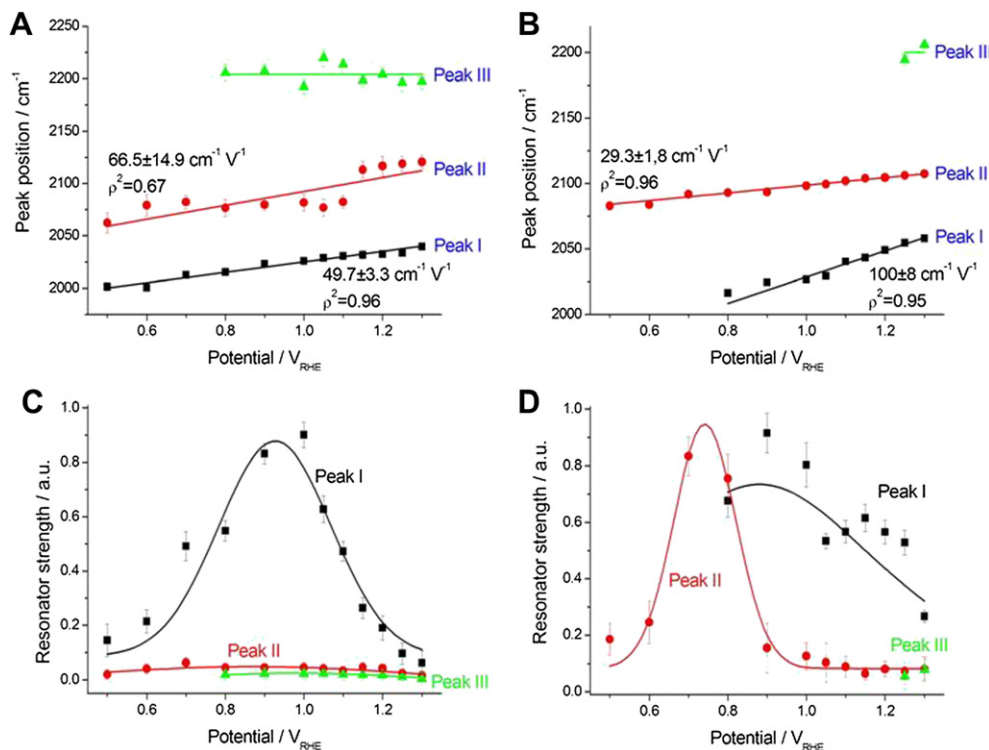
Fig. 11. Potential dependent peak positions (Panels A and B) and peak intensities (Panels C and D) derived by fitting the potential-dependent SFG spectra of Fig. 10 with the model of [18]. (A, C) Pristine sample, (B, D) aged sample.

3.5.2. Wavenumber range $1300 \div 1400$ cm^{-1}

Among the wavenumbers accessible with the FEL the chosen wavenumber range is the most diagnostic one for bands corresponding to the adsorption of ethanol and of its key oxidation products. As shown in Fig. 12, a complex spectral pattern is found, with a dominating band at $\sim 1340 \div 1345$ cm^{-1}, more prominent at less anodic potentials. This band is accompanied by a second resonance at ~ 1330 cm^{-1}, whose intensity grows with anodic polarisation. On the basis of our FTIR results (Section 3.4.2) and of the outcomes of Parts I [18] and II [19] of this investigation, we can assign: (i) the band at ~ 1330 cm^{-1} to the O=C=O asymmetric stretching of adsorbed acetate; (ii) the band at $\sim 1345/1350$ cm^{-1} to the OH and CH wagging combination of adsorbed ethanol via the C atom and to the CH_2 wagging of adsorbed ethanol via the O atom. This SFG band can thus be regarded as a fingerprint of the adsorption of undissociated ethanol.

In Fig. 13 we report potential-dependent peak positions (Panel A) and relative resonator strengths of acetate and ethanol (Panel B). A notable potential dependence is found of all peak positions: with a pristine electrode, both the ethanol (~ 1350 cm^{-1}) and acetate (~ 1330 cm^{-1}) peaks exhibit a redshift; with aged electrodes a similar, though less pronounced, trend is found with acetate, while the ethanol peak is blue-shifted in web version, denoting a change in adsorption mode. A similar scenario was found in our FTIR spectra (Section 3.4.2); in particular, both FTIR and SFG results show that both ethanol and acetate peaks exhibit an overall shift to higher wavenumbers with ageing. The resonator strength of acetate grows with anodic polarisation: this increase is better defined with the pristine catalyst than for the aged one, coherently with our FTIR findings (Fig. 8). The peak width does not exhibits a measurable potential dependence and are found to be: (i) ethanol band, pristine 6.12 ± 1.53 cm^{-1}, aged 10.19 ± 1.83 cm^{-1}; (ii) acetate
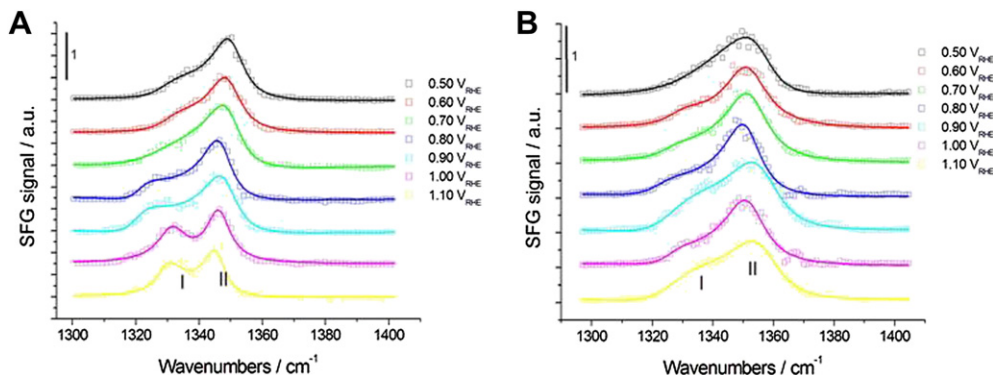

Fig. 12. Potential-dependent in situ SFG spectra measured at the indicated potentials on a WC/ECD-Pt electrode in contact with a 0.1 M $HClO_4$ + 0.1 M CH_3CH_2OH solution. Wavenumbers range corresponding to adsorbed ethanol (peak II) and its initial oxidation products (peak I). (A) Pristine sample, (B) aged sample.
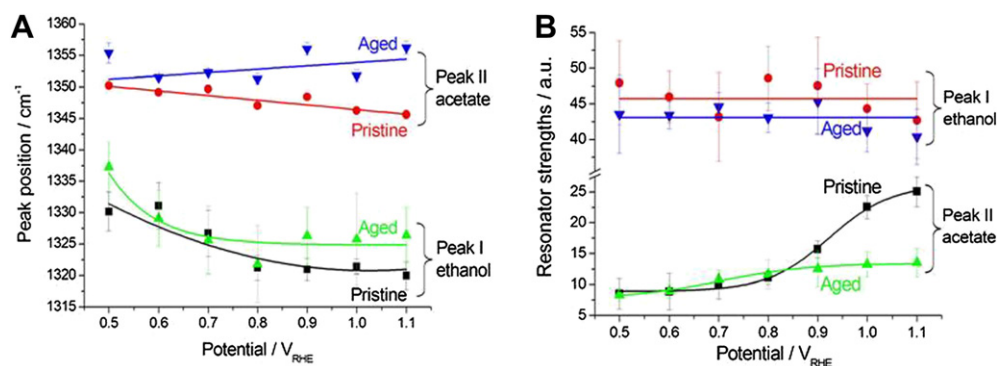
Fig. 13. Potential dependent peak positions (Panel A) and resonator strengths (Panel B) derived by fitting the potential-dependent SFG spectra of Fig. 12 with the model of [18]. The lines reported in the plots are just lines for the eye.

band, pristine 5.84 ± 1.03 cm^{-1}, aged 9.21 ± 1.14 cm^{-1}. This trend is in keeping with that found by FTIR (Section 3.4.2). The highest peak values were found with aged samples: this result can be explained with an increase in heterogeneous broadening due to the formation of multiple adsorption sites.

3.6. Scanning photoelectron microspectroscopy (SPEM)

The use of synchrotron-based SPEM and XPS with nanometric lateral resolution is motivated by the importance of gaining information about the space-dependent chemical state of Pt and W. In fact, Pt is known to be affected by operation as an electrocatalyst and WC, though working in a range of potentials in which it is cathodically protected as a single material, can be oxidatively degraded by galvanic coupling to nobler Pt.

Fig. 14. (B) SPEM micrographs of a typical location of the electrode surface recorded at the Pt 4f core level energy, highlighting the kinds of morphology brought about by electrochemical cycling (A) quasi-homogeneous background recorded at the Pt 4f energy (zone-1); (C–E) pinholes region (zone-2) recorded at the Pt 4f, W 4f and the calculated Pt/W ratio; (F–H) grain-boundary attack (zone-3).

3.6.1. Photoelectron microscopy

The key morphological features appearing as a result of electrode ageing on both micrometric and submicrometric scales have been studied by SPEM at the Pt 4f and W 4f energies (KE = 600 and 638 eV, respectively). Fig. 14B shows images of a typical region of the electrode surface; in this case, the contrast conveys both morphological and compositional information. Three different zones can be detected in this region: (i) quasi-homogeneous background, with agglomeration of Pt nanoparticles (zone-1, Fig. 14A); (ii) micrometric pinholes, corresponding to the pitting of WC grains (zone-2, Fig. 14C, see [44]); (iii) intragranular attack of the WC substrate (zone-3, Fig. 14F, see [44]). In Fig. 14A we show details of the homogeneous zone (zone-1) at higher magnifications, emphasising the granularity resulting from Pt nanoparticle agglomeration. In this area we measured local XPS spectra in various locations of a typical nanometric feature. No differences were found among survey spectra recorded in the different locations, that show the presence of Pt, C and only small amounts of W. It is worth noting that the VB spectra recorded in each position — not reported for brevity — overlap exactly. In Fig. 14 Panels C–E, we show compositional maps with typical details of the region characterised by pinholes (zone-2). Images C and D were recorded at Pt 4f and W 4f core level energies, respectively. Fig. 14E, depicted as Pt/ W, shows the ratio of Pt over W computed from the SPEM maps (C) and (D) highlighting the Pt distribution. Panels F–H of Fig. 14 report SPEM images of intergranular attack features of the WC substrate (zone-3). Fig. 14H reports the Pt/W ratio, emphasising the Pt distribution without contributions from the morphological contrast. The uncorroded surface exhibits a high Pt coverage, while Pt-rich islands are present inside the triangular hole corresponding to an attacked grain junction. This distribution explains the decrease of catalytic activity in terms of loss of Pt particles correlating with support dissolution.

3.6.2. High lateral-resolution XPS

Fig. 14 also shows a selection of representative points for micro spot XPS measurements. The local Pt 4f 7/2 and W 4f spectra are reported in Figs. 15 and 16, respectively. Deconvolution of the core-level spectra was performed with Doniach–Sunjic functions convoluted with Gaussians, accounting for the experimental resolution and broadening due to different factors [66]. In Fig. 15, the Pt 4f 7/2 peak of zone-1 shows a sizable shift from the position of clean Pt(111), that can be related to modifications of the electronic structure of metallic Pt, probably due to nanocrystallisation and agglomeration [30]. In zone-2 the selected points are A, outside the pinholes and B, inside them. The survey spectra (not shown here) show that Point B is richer in WC, while Pt is the chief constituent of
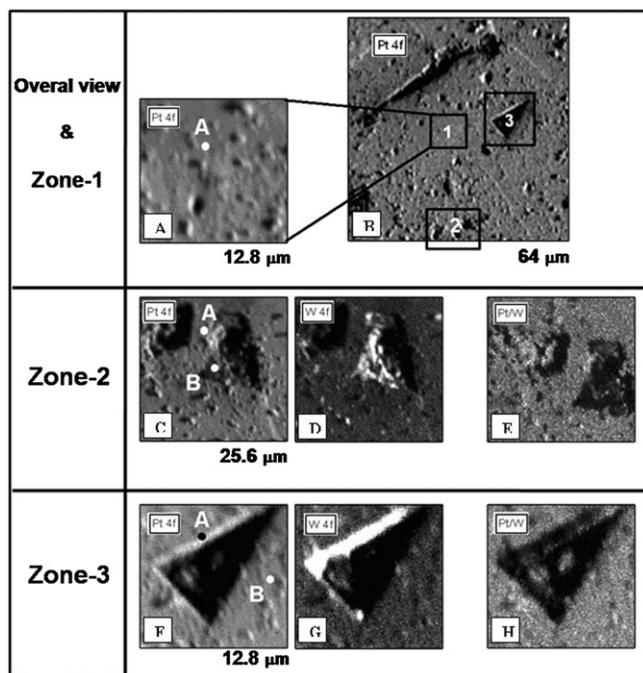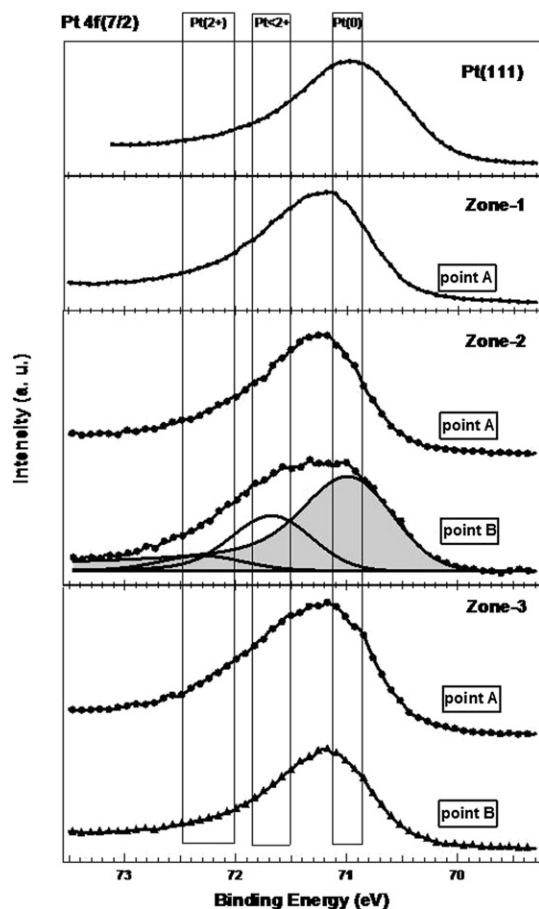
Fig. 15. Pt 4f 7/2 spectra acquired in various locations identified in Fig. 14: the "homogeneous" zone (zone-1), "Pinhole" zone (zone-2) and "intergranular attack" zone (zone-3). The Pt 4f 7/2 of Pt(111) crystal is shown for comparison as a reference.
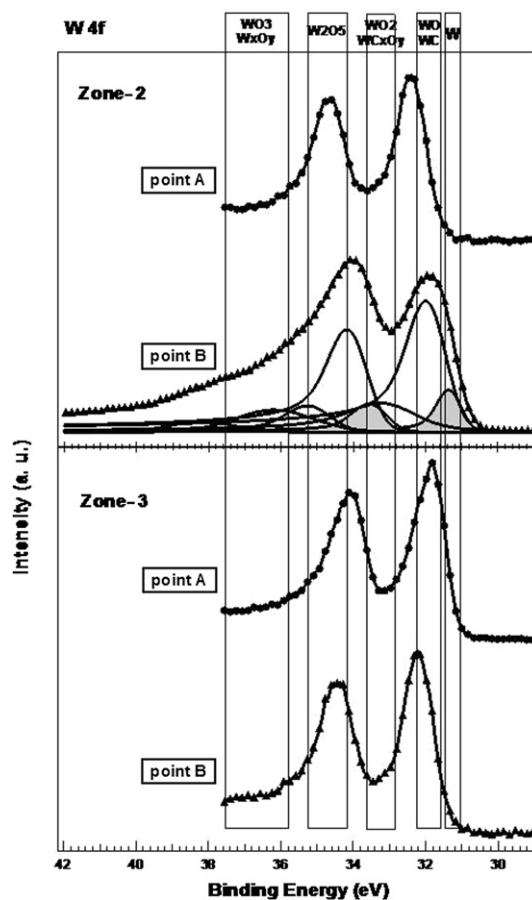

Fig. 16. W 4f spectra acquired in different points identified in panels C and F of Fig. 14: the "Pinhole" zone (zone-2) and "intergranular attack" zone (zone-3).

the surface in the other analysed points. As shown in Fig. 15, the Pt 4f 7/2 peak for point A exhibits the same components found in point A in zone-1 and shifts equally with respect to Pt(111). The spectrum corresponding to point B, instead, is quite different and its asymmetric shape has been deconvolved, disclosing the presence of small Pt(2+) and Pt(<2+) components. It is worth noting that the peak shifts with respect to Pt(111) found in this zone are to higher BEs, at variance with those found in the homogeneous zone, denoting a different chemical state of Pt(0) between the two regions. Moreover, point B, with a higher surface concentration in WC, exhibits a higher BE. In Fig. 15, we also plot the space-dependent XPS spectra recorded at the boundary of an intergranular attack feature (zone-3, point A) and close to it (point B). The Pt 4f peaks in all the analysed positions are essentially the same and are shifted equally with respect to Pt(111), coherently with the behaviour of the "pinhole" zone-2, point A.

The W 4f core level photoemission spectra acquired on the representative points A and B of zones 2 and 3, identified in Panels C and F of Fig. 14, have been summarised in Fig. 16. The asymmetric shape of the peak at point B of zone-2 denotes a remarkable difference in chemical state with respect to the other spectra. The W 4f line of the point B, inside the pinholes was deconvolved with four components: one at 31.3 eV Binding energy (BE) assigned as W metal, the main one at 32.0 eV (BE), generated by the W−C and W−O bonds, and two less intense ones at 33.1 eV and 36.4 eV (BE), respectively. These two additional components are assigned as WO_2, WC_xO_y and WO_3, W_xO_y, according to the literature [67,68].

As far as the W 4f peak is concerned, the other regions exhibit essentially the same chemical state, while the spectrum corresponding to point A zone-2 is shifted to slightly higher BE, denoting a more oxidised condition. The small contribution of W 4f corresponding to the metallic state might originate from the reducing effect of Ar^+ bombardment on partially oxidised WC, as discussed in Ref. [69]. Subtle differences in peak positions among the different points denote the chemical heterogeneity of the substrate, as expected in the vicinity of an intergranular attack feature. Overall, an anticorrelation is found between W and Pt oxidation states: this result allows a direct, space dependent, observation of the effects of galvanic coupling between nobler Pt and WC, resulting in localised corrosion. We can thus conclude that the galvanic couples, giving rise to localised attack of the substrate, develop on length scales that are smaller than the grain dimensions and thus contribute to WC attack in a way that is similar to high anodic polarisation [70].

4. Conclusions

In this paper we report an investigation into the preparation and characterisation of WC-supported electrodeposited Pt as a catalyst for ethanol anodic oxidation. WC is an appealing catalyst-support for anodic PEMFCs with improved durability. This work is a continuation of previous studies concentrating on WC-supported Pt-black [18,19]. Our research is based on electrochemical measurements, in situ FTIR and sum-frequency generation (SFG) spectroscopies of pristine and aged catalysts as well as ex situ high-resolution scanning photoelectron spectromicroscopy (SPEM). The performance of

pristine and artificially aged electrodes was compared. Cyclo-voltammetric measurements revealed a better electrocatalytic activity of WC-supported electrodeposited Pt with respect to WC-supported Pt-black. FTIR and SFG spectroscopies disclosed a rich potential-dependent spectral scenario for pristine and aged electrodes, featuring CO adsorbed in both on-top and bridge-bonded modes as well as adsorbed ethanol and acetate. Furthermore, multiple on-top CO adsorption states were disclosed by SFG, while bridge-bonded CO is present only at pristine electrodes. Oxidation of ethanol gives rise to the formation of adsorbed acetate and CO and the relative surface coverage with ethanol grows with the oxidation rate. The peak positions and Stark tuning of adsorbed CO indicate a decrease of bonding strength with ageing. The intensities and peak widths of FTIR and SFG spectra reveal multiple adsorption sites for the oxidation products (CO and acetate): evolution of the adsorption sites with ageing gives rise to a decrease and a increase of the heterogeneous broadening of adsorbed CO and acetate, respectively, correlating with a decrease of catalytic activity. Support corrosion has been shown by SPEM to give rise in parallel to W oxidation and Pt agglomeration. The position of oxidised W corresponds to that of the more reduced states of Pt, coherently with a galvanic attack mode for the substrate. The degradation of WC-supported electrodeposited Pt as an electrocatalyst for ethanol oxidation can thus be understood in terms of modifications of surface active sites and decrease of their surface concentration upon ageing, resulting in the decrease of partial oxidation of ethanol and hence increase of ethanol at the interface.

Acknowledgements

References

[1] C.G. Chung, L. Kim, Y.W. Sung, J. Lee, J.S. Chung, Int. J. Hydrogen Energy 34 (2009) 8974–8981.
[2] T. Kim, H. Lee, W. Sim, J. Lee, S. Kim, T. Lim, K. Park, Korean J. Chem. Eng. 26 (2009) 1265–1271.
[3] L. Franck-Lacaze, C. Bonnet, E. Choi, J. Moss, S. Pomtvianne, H. Poirot, R. Datta, F. Lapicque, Int. J. Hydrogen Energy 35 (2010) 10472–10481.
[4] F. Coloma, A. Sepulvedaescribano, J.L.G. Fierro, F. Rodriguez-Reinoso, Langmuir 10 (1994) 750–755.
[5] A. Guerrero-Ruiz, P. Badenes, I. Rodriguez-Ramos, Appl. Catal. A 173 (1998) 313–321.
[6] M. Kang, Y.S. Bae, C.H. Lee, Carbon 43 (2005) 1512–1516.
[7] M. Uchida, Y. Aoyama, M. Tanabe, N. Yanagihara, N. Eda, A. Ohta, J. Electrochem. Soc. 142 (1995) 2572–2576.
[8] Y. Shao, R. Kou, J. Wang, V.V. Viswanathan, J.H. Kwak, J. Liu, Y. Wang, Y. Lin, J. Power Sources 185 (2008) 280–286.
[9] M.S. Mamat, S.A. Grigoriev, K.A. Dzhus, D.M. Grant, G.S. Walker, Int. J. Hydrogen Energy 35 (2010) 7580–7587.
[10] A. Taniguchi, T. Akita, K. Yasuda, Y. Miyazaki, Int. J. Hydrogen Energy 33 (2008) 2323–2329.
[11] D.A. Stevens, J.R. Dahn, Carbon 43 (2005) 179–188.
[12] J.P. Meyers, R.M. Darling, J. Electrochem. Soc. 153 (2006) A1432–A1442.
[13] T. Yoda, H. Uchida, M. Watanabe, Electrochim. Acta 52 (2007) 5997–6005.
[14] C.H. Paik, G.S. Saloka, G.W. Graham, Electrochem. Solid State Lett. 10 (2007) B39–B42.
[15] J. Wang, G. Yin, Y. Shao, Sh. Zhang, Zh. Wang, Y. Gao, J. Power Sources 171 (2007) 331–339.
[16] R.L. Whetten, D.M. Cox, D.J. Trevor, A. Kaldor, Phys. Rev. Lett. 54 (1985) 1494–1497.
[17] R.R. Adzic, J. Wang, B.M. Ocko, Electrochim. Acta 40 (1995) 83–89.
[18] B. Bozzini, G.P. De Gaudenzi, B. Busson, Ch. Humbert, C. Six, A. Gayral, A. Tadjeddine, J. Power Sources 195 (2010) 4119–4123.
[19] B. Bozzini, G.P. De Gaudenzi, A. Tadjeddine, J. Power Sources 195 (2010) 7968–7973.
[20] D.R. McIntyre, G.T. Burstein, A. Vossen, J. Power Sources 107 (2002) 67–73.
[21] G. Lu, J.S. Cooper, P.J. McGinn, J. Power Sources 161 (2006) 106–114.
[22] C.D.A. Brady, E.J. Rees, G.T. Burstein, J. Power Sources 179 (2008) 17–26.
[23] H. Chhina, S. Campbell, O. Kesler, J. Power Sources 164 (2007) 431–440.
[24] F.P. Hu, P.K. Shen, J. Power Sources 173 (2007) 877–881.
[25] C. Bianchini, P.K. Shen, Chem. Rev. 109 (2009) 4183–4206.
[26] H. Meng, P.K. Shen, Chem. Commun. (2005) 4408–4410.
[27] Z. Hu, M. Wu, Z. Wei, Sh. Song, P.K. Shen, J. Power Sources 166 (2007) 458–461.
[28] M. Nie, H. Tang, Z. Wei, S.P. Jiang, P.K. Shen, Electrochem. Commun. 9 (2007) 2375–2379.
[29] F. Hu, G. Cui, Z. Wei, P.K. Shen, Electrochem. Commun. 10 (2008) 1303–1306.
[30] B. Bozzini, M. Amati, M. Boniardi, M. Kazemian Abyaneh, L. Gregoratti, M. Kiskinova, J. Power Sources 196 (2011) 2513–2518.
[31] B. Bozzini, M. Amati, M. Kazemian Abyaneh, L. Gregoratti, M. Kiskinova, J. Electroanal. Chem. 657 (2011) 113–116.
[32] M. Paunovic, M. Schlesinger, Fundamentals of Electrochemical Deposition, Wiley, New York, 1998.
[33] N. Saibuatong, Y. Saejeng, K. Pruksathorn, M. Hunson, N. Tantavichet, J. Appl. Electrochem. 40 (2010) 903–910.
[34] H. Kim, B.N. Popov, Electrochem. Solid State Lett. 7 (2004) A71–A74.
[35] H. Kim, N.P. Subramanian, B.N. Popov, J. Power Sources 138 (2004) 14–24.
[36] E.J. Taylor, E.B. Anderson, N.R.K. Vilambi, J. Electrochem. Soc. 139 (1992) L45–L46.
[37] Y. Ra, J. Leeb, I. Kim, S. Bong, H. Kim, J. Power Sources 187 (2009) 363–370.
[38] N. Rajalakshmi, K.S. Dhathathreyan, Int. J. Hydrogen Energy 33 (2008) 5672–5677.
[39] S.D. Thompson, L.R. Jordan, M. Forsyth, Electrochim. Acta 46 (2001) 1657–1663.
[40] S. Lertviriyapaisan, N. Tantavichet, Int. J. Hydrogen Energy 35 (2010) 10464–10471.
[41] J.M. Rheaume, B. Müller, M. Schulze, J. Power Sources 76 (1998) 60–68.
[42] A. Taniguchi, T. Akita, K. Yasuda, Y. Miyazaki, J. Power Sources 130 (2004) 42–49.
[43] L. Gregoratti, A. Barinov, E. Benfatto, G. Cautero, C. Fava, P. Lacovig, D. Lonza, M. Kiskinova, R. Tommasini, S. Mahl, Rev. Sci. Instrum. 75 (2004) 64–69.
[44] B. Bozzini, M. Dalmiglio, G.P. De Gaudenzi, L. D'Urzo, L. Gregoratti, Corros. Sci. 51 (2009) 1675–1678.
[45] S.S. Gupta, J. Datta, J. Electroanal. Chem. 594 (2006) 65–72.
[46] S. Park, Y.Y. Tong, A. Wieckowski, M.J. Weaver, Electrochem. Commun. 3 (2001) 509–513.
[47] T. Iwasita, F.C. Nart, in: H. Gerischer, C.W. Tobias (Eds.), Advances in Electrochemical Science and Engineering, vol. 4, 1995, pp. 169–171, Weinheim.
[48] T. Iwasita, B. Rasch, E. Cattaneo, W. Vielstich, Electrochim. Acta 34 (8) (1989) 1073–1079.
[49] P. Gao, S.C. Chang, Z. Zhou, M. Weaver, J. Electroanal. Chem. 272 (1989) 161–178.
[50] F.H.B. Lima, E.R. Gonzalez, Electrochim. Acta 53 (2008) 2963–2971.
[51] J.F.E. Gootzen, W. Visscher, J.A.R. van Veen, Langmuir 12 (1996) 5076–5082.
[52] E. Antolini, J. Power Sources 170 (2007) 1–12.
[53] T. Iwasita, F.C. Nart, Prog. Surf. Sci. 55 (1997) 271–340.
[54] F. Liu, M. Yan, W. Zhou, Z. Jiang, Electrochem. Commun. 5 (2003) 276–282.
[55] B. Bozzini, C. Mele, A. Fanigliulo, B. Busson, F. Vidal, A. Tadjeddine, J. Electroanal. Chem. 574 (2004) 85–94.
[56] S.-C. Chang, M.J. Weaver, J. Phys. Chem. 95 (1991) 5391–5400.
[57] B. Bozzini, L. D'Urzo, V. Romanello, C. Mele, J. Electrochem. Soc. 153 (2006) C254–C257.
[58] D. Curulla Ferré, J.W. Niemantsverdriet, Electrochim. Acta 53 (2008) 2897–2906.
[59] J.F. Gomes, B. Busson, A. Tadjeddine, J. Phys. Chem. B 110 (2006) 5508–5514.
[60] J. Fernandes Gomes, B. Busson, A. Tadjeddine, G. Tremiliosi-Filho, Electrochim. Acta 53 (2008) 6899–6905.
[61] A. Peremans, A. Tadjeddine, J. Electroanal. Chem. 395 (1995) 313–316.
[62] F. Vidal, B. Busson, C. Six, O. Pluchery, A. Tadjeddine, Surf. Sci. 502–503 (2002) 485–489.
[63] F. Vidal, B. Busson, C. Six, A. Tadjeddine, L. Dreesen, C. Humbert, A. Peremans, P. Thiry, J. Electroanal. Chem. 563 (2004) 9–14.
[64] F. Vidal, B. Busson, A. Tadjeddine, Chem. Phys. Lett. 403 (2005) 324–328.
[65] B. Bozzini, B. Busson, G.P. De Gaudenzi, L. D'Urzo, C. Mele, A. Tadjeddine, J. Electroanal. Chem. 602 (2007) 61–69.
[66] S. Doniach, M. Sunjic, J. Phys. C 3 (1970) 285–291.
[67] J. Brillo, H. Kuhlenbeck, H.-J. Freund, Surf. Sci. 409 (1998) 199–206.
[68] K. Mašek, J. Libra, T. Skála, M. Cabala, V. Matolín, V. Cháb, K.C. Prince, Surf. Sci. 600 (2006) 1624–1627.
[69] A. Katrib, F. Hemming, P. Wehrer, L. Hilaire, G. Maire, Catal. Lett. 29 (1994) 397–408.
[70] B. Bozzini, G.P. De Gaudenzi, A. Fanigliulo, Corros. Sci. 46 (2004) 453–469.